**Neuron, Volume *75***
**Supplemental Information**

# Traveling Theta Waves along the Entire Septotemporal Axis of the Hippocampus

**Jagdish Patel, Shigeyoshi Fujisawa, Antal Berényi, Sébastien Royer, and György Buzsáki**

## Supplemental Experimental Procedures

### Animals and chronic surgery

Data were collected from 12 Long-Evans rats (male, 250-400g, 3-5 months old). The details of surgery and recovery procedures used have been described earlier (Csicsvari et al. 1998). In brief, animals were deeply anesthetized with isoflurane and up to four separate craniotomies were performed over the right hippocampus. In 7 rats, two separate drives were implanted for electrophysiological recordings; one targeted the septal-intermediate 2/3$^{rd}$ and the other the ventral (4$^{th}$ quadrant) CA1 pyramidal layer. In the 8th rat (rat-11), the drive targeted only the septal 2/3 CA1 pyramidal layer. In the 9$^{th}$ rat (r-27), the septal drive was placed along the transverse axis in order to record activity along the subiculum-CA1-CA2-CA3 axis. In 2 additional rats (rat-29 & rat-30), 4 silicon probes (each with 8 vertical sites x 4 shanks; 20μm vertical site separation and 200μm intershank interval; shanks of each probe were placed along the transverse axis while the probes were placed along the longitudinal axis, see Fig 4A inset) were implanted in order to record the physiological activity in 3-D. In one rat (r-tn), a 256-site probe (32 sites on each of the 8 shanks with 50μm vertical site separation and 300 μm intershank interval) was implanted perpendicular to the long axis of the dorsal hippocampus. This high-density probe was used to examine the theta phase shift in the CA1-CA3 pyramidal layer. The electrodes, up to 10, (tetrodes made from 12.5 μm nichrome wires, 6 rats; Royer et al., 2010 or single 50 μm tungsten wires, 3 rats) for recordings from the dorsal-intermediate CA1 segments were organized in a straight line and spanned upto 6.5 mm distance along the curvature of the CA1 pyramidal layer. These arrays were inserted parallel with the long axis of the hippocampus so that the tips arrived in the CA1 pyramidal layer at approximately the same distance from the subicular and CA3 borders at all septo-temporal levels. Ventral recordings were made with either tetrodes (2 rats) or single 50 μm wires (2 rats) or silicon probes (8 sites x 4 shanks, 6 rats; Royer et al., 2010). The high-density 32-site silicon probe had 4-shanks with 'octrode' design (20-μm vertical site spacing in each shank and 200-μm inter-shank distance; NeuroNexus Technologies, MI; Royer et al., 2010). All tetrodes and single wires were independently movable. The septal drive/s was/were placed between AP: 2.2 to 6.3 and ML: 0.8 to 6.0 while the ventral drive between AP: 4.5 to 6 and ML: 4 to 5.7. Prior to implantation, the electrode tips were gold-plated to reduce electrode impedances to ~300 kΩ at 1 kHz. Recordings, with tetrodes in 1 rat (r-27) and with multiple shank probes in 4 rats (r-tn, r-jc, r-s1 and r-s2) were used for theta wave analysis along the subiculo-fimbrial axis, 3 of which (r-jc, r-s1 and r-s2) were used in previous publications (Csicsvari et al., 2003; Montgomery et al., 2009). In all experiments, ground and reference screws were implanted in the bone above the cerebellum. After post-surgical recovery, recording wires were lowered over the course of several days in steps of 50 μm until large units and ripple activity were isolated at appropriate depths. The goal was to record, simultaneously, from at least 3 sites in the dorsal/intermediate CA1 pyramidal layer along the long axis, and at least 1 from the CA1 pyramidal

layer in the ventral pole (except 2 rats (r-27 and r-tn), in which recordings were obtained only along the transverse axis). All experiments were carried out in accordance with protocols approved by the Institutional Animal Care and Use Committee, Rutgers University.

**Behavioral training**

All animals were handled and trained in two mazes (an open field and a zigzag maze) for at least two weeks before surgery (Royer et al., 2010). The animals were water-restricted for 24 h before the tasks. The same behavioral procedures were used for training and testing. The apparatus was separated from the experimenter and recording equipment by a black curtain, which also served as a polarizing cue relative to the walls on the other two sides. The floor and walls of the mazes were washed between sessions.

*Open maze*. The animals were trained to forage for small pieces (~3 x 3 mm) of froot loops (Cereal Kelloggs) on the open maze (114 x 184 cm) thrown one at a time from behind a curtain. The open maze had 30 cm high side-walls on all 4 sides, tilting outward by $60^{o}$. The entire maze was painted black. The rat could freely see distant room cues.

*Zigzag maze*. By placing 5 roof-shaped partitioning walls into the open maze, it was converted into a zig-zag maze with 11 corridors. The walls were 30 cm high with a 24 cm base and painted black. The animals were trained to run back and forth between the 2 water wells, situated in the end compartments. 100 µl of water was delivered at each well, alternatively (Royer et al., 2010).

*Homecage*: All sleep sessions were recorded while the rats slept or were inactive in their homecage. Sleep sessions were recorded at the beginning of each day followed by a behavioral session, followed by more sleep sessions. Sleep sessions were terminated if the rat awakened and moved and continued only after a minimum waiting period of 15 minutes and when it returned to uninterrupted inactivity/sleep for at least 5 minutes.

**Histological and physiological verification of recording sites**

Since the main goal of the present experiments was to establish theta phase relationships among signals recorded along the LA of the hippocampus, the physical distances between the recording sites rather than the stereotaxic coordinates of the electrodes were used for comparing physiological features of theta waves. In 2 separate rats, the hippocampi were removed following decapitation and placed in ice-cold cerebro-spinal fluid. The hippocampus was gently flattened and the distance between the anterior (septal) and posterior (temporal) poles was measured. In agreement with previous similar measurements (Amaral and Lavenex, 2007), the septo-temporal length of the adult hippocampus was approximately 10 mm. In all figures, the distances of the electrodes are given from the septal end of the hippocampus (e.g., Figure 2). These distances were determined from anatomically verified sites of the electrodes and the extrapolated distance of the stereotaxic coordinates of the electrode position from the septal pole (Paxinos and Watson, 1996), taking into account the curvature of the hippocampus (Figures 2A and 2B).

The electrode tracks of both wire electrode and silicon probe shanks were determined from the histological sections. To identify the exact location of the recording sites, a small anodal current (5 µA for 10 sec) was passed through the recording electrodes 2 days prior to sacrificing the animals (Fujisawa et al., 2008). The rats were deeply anesthetized and perfused through the heart: first with 0.9% saline solution and followed by 10% formalin solution. The brains were sectioned by a Vibratome (Leica,

Germany) at 100 μm, either along the longitudinal, transverse or coronal plane. Sections were mounted on the slides, Nissl stained, and cover-slipped. The tracks were typically reconstructed from multiple adjacent sections.

Since silicon probes have a fixed geometry, the recording sites can unambiguously inform the experimenter whether the sites are above, in or below the pyramidal layer with 20-μm precision (within a 140 μm span; e.g., Mizuseki et al., 2011), i.e., better than what can be established by lesioning the sites (Fujisawa et al., 2008). Due to the fixed geometry of the recording sites and shank distances, the relative depths of the recording sites can be reliable determined even if only one unambiguous histological verification is available for only one or two shanks (Csicsvari et al., 2003; Montgomery et al., 2009; Mizuseki et al., 2011). Within the CA1 pyramidal layer, the electrodes were advanced until sharp wave-ripples, associated with unit firing in the CA1 pyramidal layer, were detected during sleep in the home cage. During subsequent recording sessions, the electrodes were further adjusted to obtain largest amplitude ripples, corresponding to the middle of the pyramidal layer (Mizuseki et al., 2011). To facilitate visual comparison of the recording sites and LFP events, the silicon probe tips were superimposed on the histological sections (e.g., Figures 1, S1, S2 and S3).

Only data with verified electrode tracks and physiological recordings of ripples and unit firing were included in the analyses. Due to these strict criteria, data obtained from 29 dorsal/intermediate sites and 17 ventral sites were excluded from further analysis because the electrode tracks were outside the CA1 pyramidal layer (in CA1 radiatum, CA2, subicular region) or because the tracks could not be verified reliably. Occasionally, the electrodes moved the tissue a bit deeper. Such tissue 'dragging' was observed mainly with blunt single wire electrodes and tetrodes, appearing as indentation of the pyramidal cell layer (e.g., Figure 2A, S2A and S3B). In the dorsal (septal) hippocampus, pushing the pyramidal layer into the stratum radiatum, in principle, could lead to an artificial theta phase measure reducing the magnitude of the D-V phase shift. There are two arguments against the effects of tissue dragging in our experiments. First, the theta phase shift below the pyramidal layer is gradual and reaches ~$90^{o}$ in mid-radiatum (Winson, 1974). Such large indentation has never been observed. Second, the middle of the pyramidal layer was determined by the maximum of ripple power (Mizuseki et al., 2011). This latter observation would suggest that even if the pyramidal layer is moved deeper, most of the LFP activity still reflects the nearby current sources, i.e., the pyramidal layer.

**Data acquisition, processing and analysis**

During the recording session the rat was connected to a light-weight, counter-balanced cable that allowed the animal to move freely in the apparatus or to sleep comfortably in the homecage. During the recording sessions, neurophysiological signals were amplified (1,000 X), band pass filtered (1 Hz - 9 kHz), acquired continuously at 32 kHz on a 128-channel DigiLynx System (24-bit resolution; NeuraLynx, MT) and stored for offline analysis. Raw data were preprocessed using custom-developed suite of programs (Csicsvari et al., 1998). The wide-band signal was low pass filtered and down sampled to 1252 Hz to generate the local field potential (LFP) and was high-pass filtered (>0.8 kHz) for spike detection. For tracking the position of the animals, two small light emitting diodes, mounted above the headstage, were recorded by a digital video camera and sampled at 30 Hz. Malfunctioning recording sites (due to high impedence, cross-talk, short circuit) or sites without large units and ripples were removed from the analysis.

*Spike sorting and cell classification.* Spike sorting was performed offline using a semiautomatic,

custom-developed clustering analysis program (http://klustakwik.sourceforge.net; Harris et al., 2000), followed by manual adjustment of unit clusters, aided by autocorrelation and cross-correlation functions as additional separation tools (http://klusters.sourceforge.net; http://neuroscope.sourceforge.net; Hazan et al., 2006). Only clusters with clear refractory periods and well-defined boundaries in at least one of the projections were included in the single unit analysis (Harris et al, 2000). The tip of the electrodes either moved spontaneously between sessions or was moved by the experimenter. We cannot exclude the possibility that some neurons recorded in different sessions were partially overlapping because spikes from each session were clustered separately.

*Detection of theta periods*: Theta periods were detected automatically using the ratio of the power in the theta band (5-10 Hz) to the power of the nearby bands (1-4 Hz, 12-15 Hz) from either the most dorsal or the most ventral CA1 sites in each rat. This was followed by manual adjustment based on the visual inspection of whitened power spectra (using a low-order autoregressive model; Mitra and Pesaran, 1999) and the raw EEG (Sirota et al, 2008). The manual adjustment was especially necessary in behavioral sessions to remove the falsely detected short segments containing movement artifacts. Theta periods of duration <4 seconds for REM periods and <2 seconds for RUN sessions were further removed. Theta periods, detected in both behavioral and sleep/inactivity sessions, were analyzed further.

*Spectral Analysis*: Detected theta periods were concatenated to form a continuous signal and whitened using an autoregressive model, using a 1-second window. The autoregressive model generated from the 1$^{st}$ channel was then re-used for whitening all other channels from the same session in order to maintain the scale. Signals thus produced were used for the measurement of power. All coherence estimates and phase estimates were performed from non-whitened signal. All spectral analysis employed multitaper direct spectral estimates method. Since our analysis was focused on the theta frequency band, we used a window size of 1 second with 5 tapers. Phase shifts along the septo-temporal axis were measured taking the most ventrally located channel as reference, while phase shift along the subiculo-fimbrial axis was measured taking the most distally located CA1 site as the reference channel (Figure S3).

*Theta amplitude and phase*: LFP from all channels was theta filtered between 5-10 Hz using a Butterworth filter with a 1-second window. Instantaneous amplitude and phase of theta oscillations were derived from Hilbert transformation of the filtered LFP trace, following Siapas et al. (2005). Local minima were detected from the filtered signal of the reference channel to generate trough-triggered field averages for all channels. Multiple unit activity was extracted from all channels (Figure 3). Instantaneous phase of the local channel was used to assign theta phases to spikes (Figure 3).

*Unit Analysis*: Because single units cannot be reliably identified from single wire recordings (Harris et al., 2000), and because we wanted to generate group data from all rats, unit firing vs. theta phase relationship was first analyzed for multiple unit data. Multiple unit was obtained by removing the noise cluster from the data and combining all spikes into a single spike series. Single units were identified from the ventral recording sites and segregated into putative pyramidal cells or interneurons, based on firing rates. Cells with firing rates <5 Hz were classified as putative pyramidal cells and all others as putative interneurons (Royer et al., 2010). Only single units with at least 100 spikes and a firing rate of >.1 Hz were used to test their phase locking. Rayleigh test for the uniformity of the phase of firing was used to identify phase-modulated pyramidal cells. Pyramidal cells with a P value of <0.05 were considered to be significantly phase-locked (Figure 3).

*Permutation test*: A permutation test was used to assess the statistical significance of the difference of theta phase shift slopes between different brain states (i.e. REM and RUN). First, the regression coefficients between phase shifts and anatomical distances were calculated for data from each brain state, using a multiple linear regression model. Second, to form the surrogate data sets, each label (i.e. REM and RUN) of each data point in the original data set was randomly shuffled. Next, the regression coefficients were estimated for these surrogate data sets and the difference of slopes for the two states was noted. This process was repeated independently to generate 10,000 counts of slope differences. Finally, the phase shift difference between REM and RUN were determined to be statistically significant if they were atypical with respect to those constructed from the shuffled data sets (Figure 2).

## Supplemental Information (Figures S1-S6)

Figures and figure legends

Figure S1 provides histological information relevant to Figures 1-5.
Figure S2 describes theta phase changes along the transverse axis . Complements Figures 1 and 3.
Figure S3. Single rat example of theta phase shift in the dorsal-intermediate CA1. It provides additional information to Figure 2.
Figure S4. Example of dorsal vs ventral theta features. It provides additional information to Figure 1, 2, 3 and 5.
Figure S5. Traveling theta waves along the septo-temporal axis. This figure is complementary to Figure 3.
Figure S6. It provides additional information to Figure 3. It compares the slope of phase shift calculated only from sites in septal 2/3$^{rd}$ with sites it the entire hippocampus.

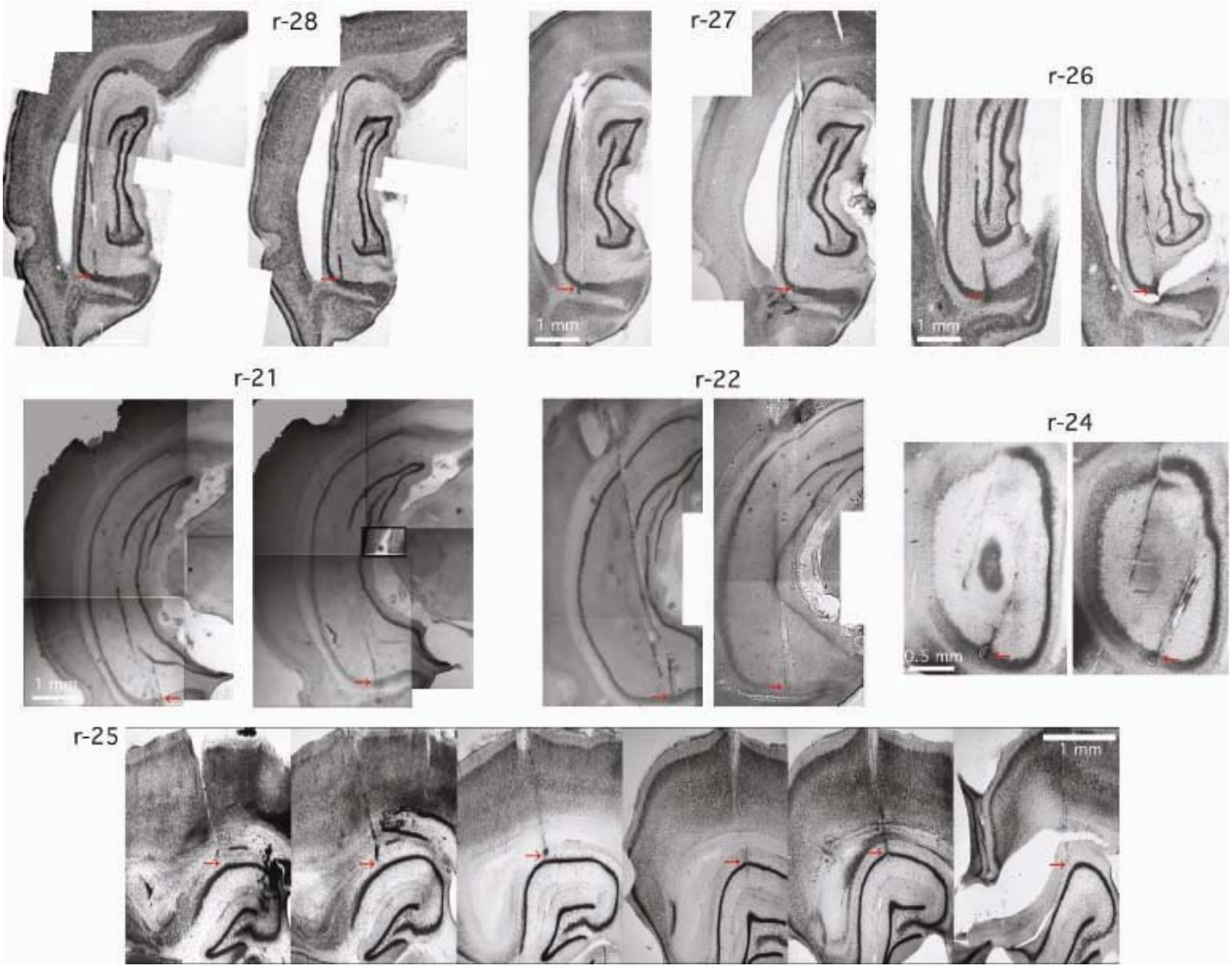


**Figure S1. Histological reconstruction of the recording tracks.** Red arrows indicate the extrapolated or verified (lesion) tip. Every rat has at least one clearly identified lesion site. All rat brains were sectioned along the transverse axis i.e. axis perpendicular to the LA, except of rat r-24 which was cut in the coronal plane. The distance between the first and last recording electrode in r-25 is 4.5 mm (0.9 mm gaps between electrodes). This figure provides supplementary information to Figures 1-5.

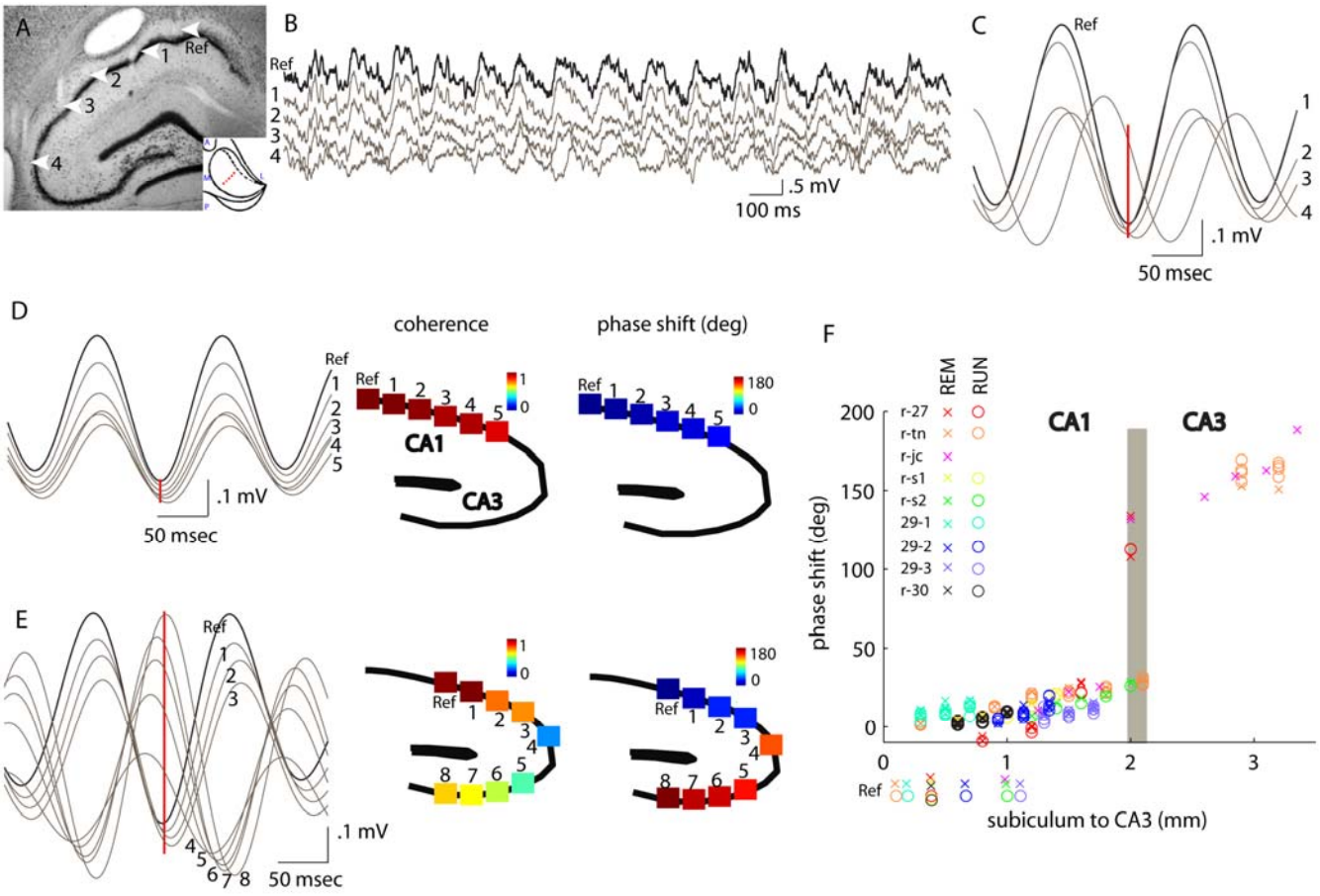


**Figure S2. Theta phase shift in the subiculo-fimbrial axis**. (A) Histological reconstruction of 5 tetrode tracks in the subiculo-fimbrial axis (reference, Ref and 1-4; rat-27). Sections were cut along the transverse axis of the hippocampus. Inset: Top-down view of the right hippocampus illustrating tetrode placement along the transverse axis. (B) Two-second long wide-band LFP traces during theta from the sites shown in A. (C) Average filtered (5–10 Hz) theta waves during RUN from the same recording sites as in A and B. (D) left: Average filtered theta waves during RUN. middle and right: coherence and phase shift against the most medial reference (Ref) site. Note phase-shifted theta waves in the CA1 pyramidal layer along the subiculo-fimbrial axis relative to the most distal (subicular) CA1 reference. Silicon probe recordings with 300 μ intershank distance (r-sm2). (E) Same as in D from another rat (r-jc) equipped with a 96-site silicon probe (REM). Note large phase shifts of theta waves between the CA1 and CA3 sites. (F) Group data of phase shifts during REM (X) and RUN (O). Different colors code for different rats. Reference locations are shown below the x axis. Note moderate phase shift in the subiculo-fimbrial axis of CA1 pyramidal layer and phase reversal of theta waves between CA1 and CA3. This figure complements Figures 1 and 3.

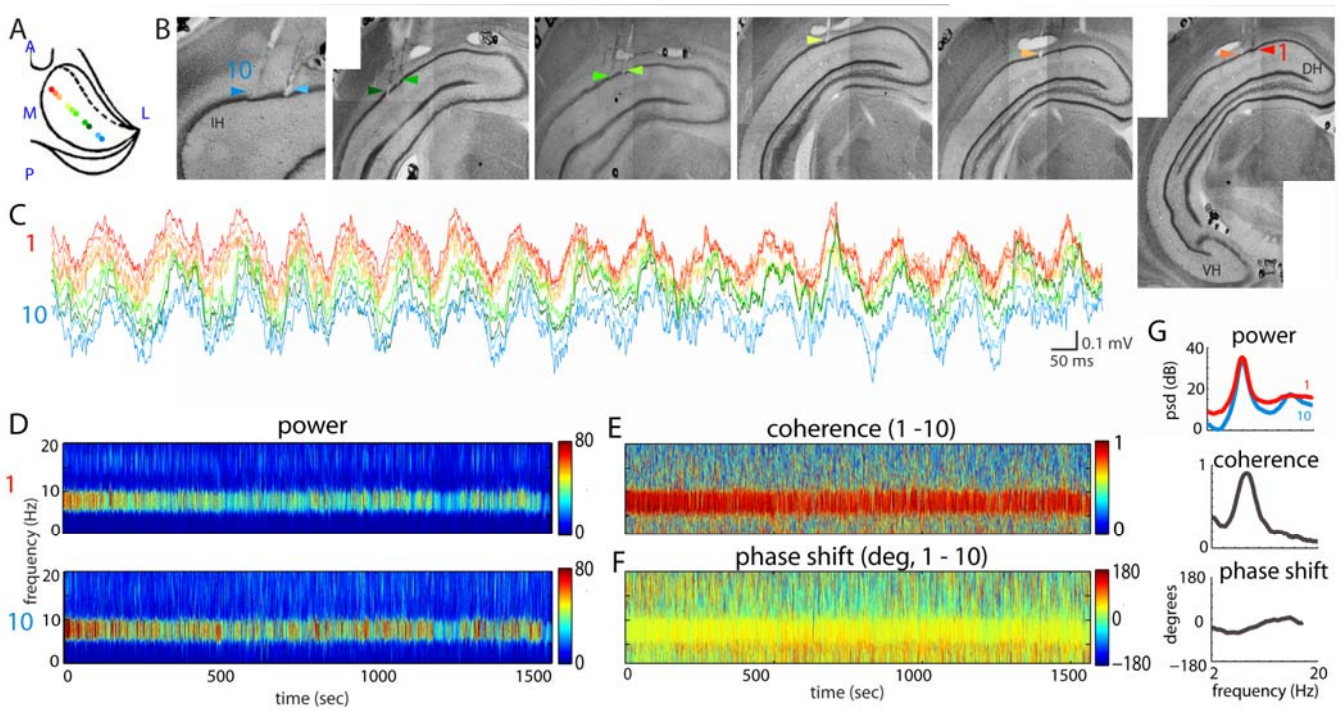


**Figure S3. Theta oscillations in the dorsal and intermediate hippocampus.** (A). Top-down view of the right hippocampus illustrating electrode placement along the long axis. Each colored dot indicates one electrode. (B) Histological sections showing ten recordings sites from the dorsal (DH) and intermediate (IH) parts of the CA1 pyramidal layer (r-11). Sections were cut parallel with the LA of the hippocampus. Arrowheads, tips of the electrodes. Color-coding of the electrodes applies also to parts B, C, D and G. (C) Two-second long wide-band LFP traces during RUN theta from all recording locations. (D). Time-resolved power spectra during run periods concatenated over the entire session, from the most septal (dorsal) and intermediate electrodes. Coherogram (E) and time-resolved phase (difference) spectra (F) calculated between channels shown in D. (G) Average power, coherence and phase spectra for the sites shown in D. Phase is shown where coherence is >0.1. This figure is supplementary to Figure 2.

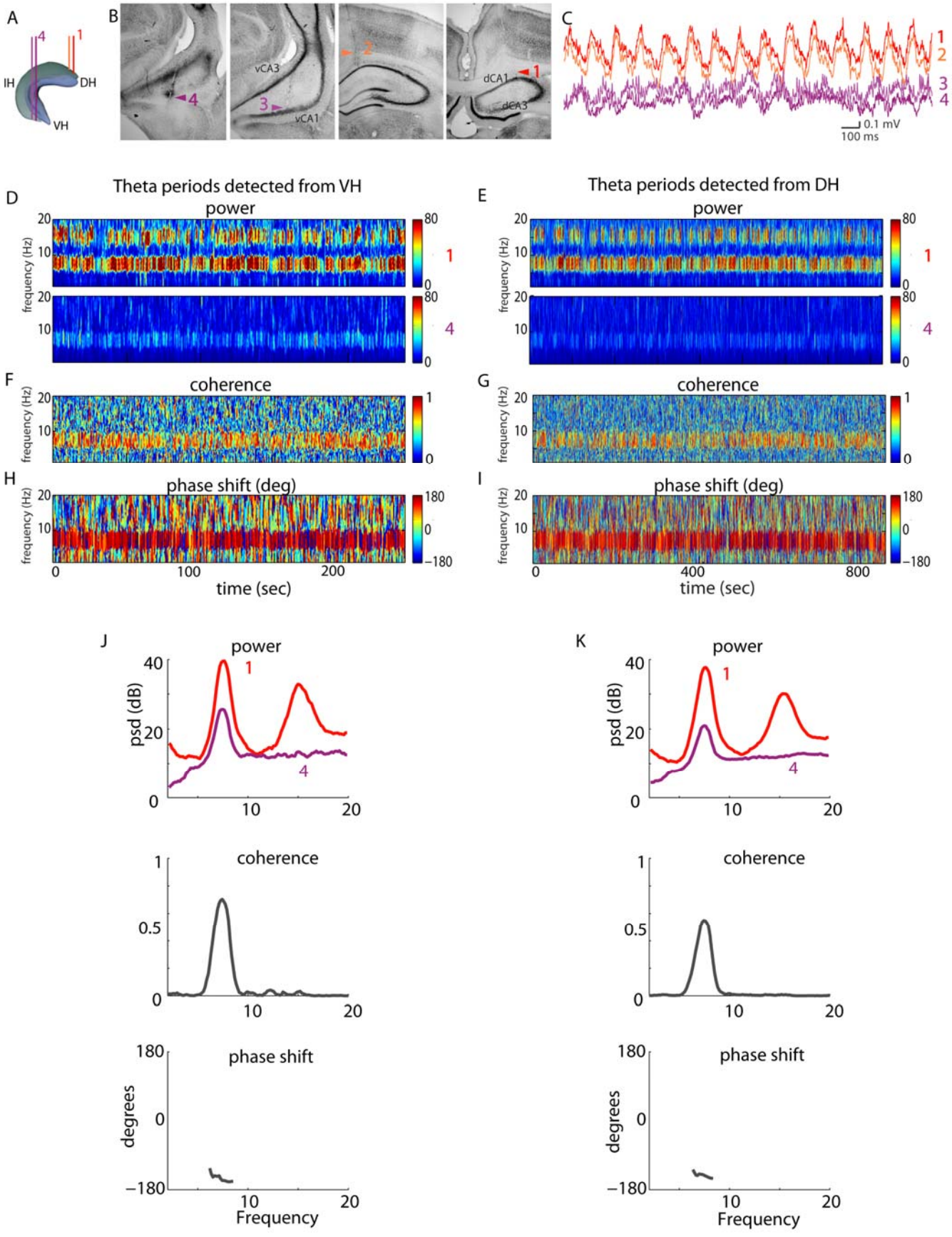
A
4
1
IH
DH
VH
B
vCA3
3
vCA1
2
dCA1
1
dCA3
4
C
1
2
3
4
0.1 mV
100 ms
D
Theta periods detected from VH
power
frequency (Hz)
20
10
80
0
1
4
E
Theta periods detected from DH
power
F
coherence
1
0
G
coherence
H
phase shift (deg)
180
0
−180
0
100
200
time (sec)
I
phase shift (deg)
0
400
800
time (sec)
J
power
psd (dB)
40
20
0
10
20
coherence
0.5
phase shift
degrees
Frequency
K
power
coherence
phase shift

**Figure S4. Largely independent amplitude variability in the DH and VH. (**A). Schematics of the recording sites in the dorsal and ventral segments of the hippocampus (r-23). Color-coding of recording sites also applies to traces in parts B and C. (B). Transverse sections (cut perpendicularly to the LA) showing two recording sites in the ventral and two sites in the dorsal CA1 pyramidal layer. (C) A short segment of LFP during RUN. Note approximately half cycle (180$^o$) phase shift of theta oscillations between the most dorsal and most ventral CA1 pyramidal layers. (D, F, H) Time-resolved power, coherence and phase spectra for RUN theta periods, referenced to theta epochs detected from the ventral hippocampal site (VH). (J) Average power, coherence and phase spectra (E, G, I, K) Same as D, F, H and J but theta epochs were detected from the dorsal hippocampal site (DH). Note reduced theta power in the VH and lower theta coherence when theta periods are detected from DH. Note also that reference theta site selection bias does not affect theta phase difference (Phase shift is shown only when coherence is >0.1). This figure is supplementary to Figures 1, 2, 3 and 5.

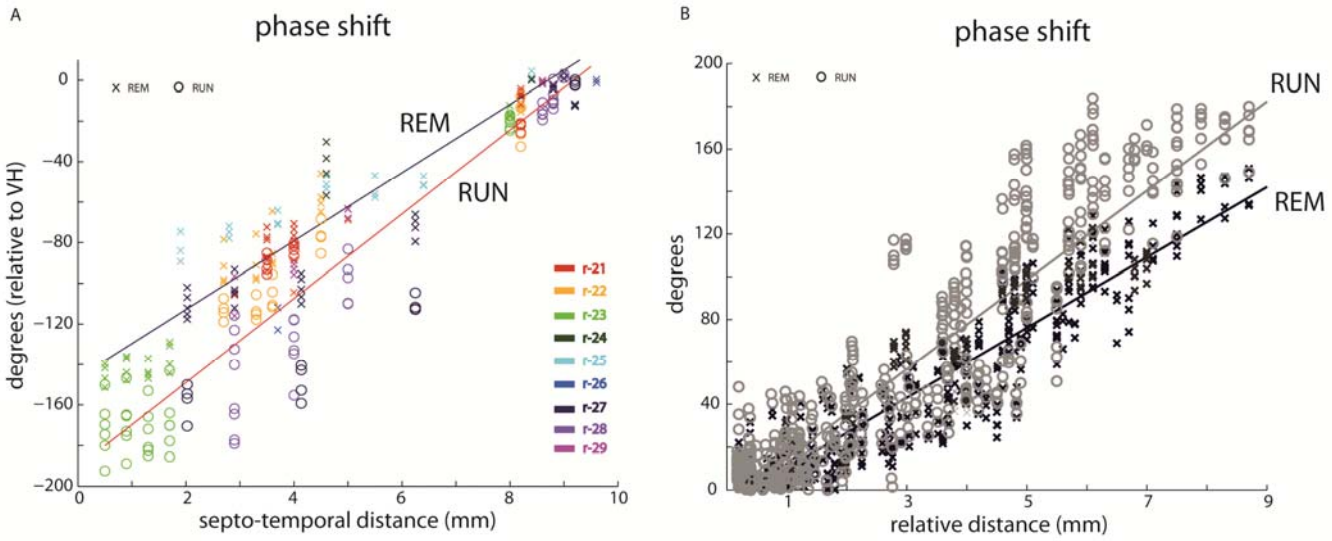


**Figure S5. Traveling theta waves along the septo-temporal axis.** Here, theta epochs were selected from the recordings from the dorsal hippocampus (in Figure 3, the inclusion criterion was the presence of thresholded theta power from the ventral hippocampus). (A). Phase shift of theta oscillations in single rats (color symbols) as a function of septo-temporal distance. Note up to 180$^o$ phase shift between the ventral-most and septal-most (dorsal) sites during RUN and significantly less steep phase shift during REM. (B). Theta phase shift as a function of electrode distance. All possible electrode pair comparisons (relative distance) are shown. This figure is supplementary to Figures 3F and 3G, respectively.

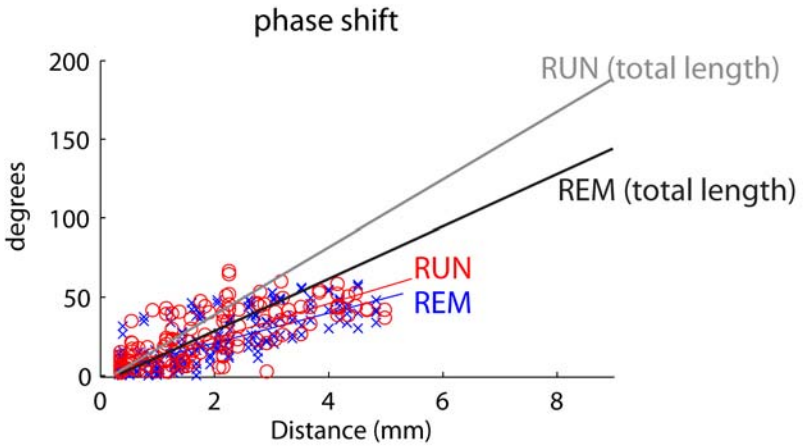


**Figure S6. Discontiguity of theta coherence between intermediate and ventral segments of the hippocampus.** Phase shift slopes measured separately for data points in the septal 2/3rd alone compared to data along the whole long axis. Note that the slope of theta phase vs distance from ONLY septal data is less steep compared to the slope obtained from data all along the LA (gray lines). This difference suggests that the speed of theta wave travel is slower in the septal-intermediate segments of the hippocampus and accelerates between the intermediate and ventral segments. This figure is supplementary to Figure 2.

**Supplemental References**

Amaral, D., and, Lavenex, P. (2007). Hippocampal Neuroanatomy in: *The Hippocampus Book*. P. Andersen, R. Morris, D. Amaral, T. Bliss, J. O'Keefe, eds. (New York: Oxford University Press).

Csicsvari, J., Hirase, H., Czurko, A., and Buzsáki, G. (1998). Reliability and state dependence of pyramidal cell-interneuron synapses in the hippocampus: an ensemble approach in the behaving rat. Neuron. 21, 179-89.

Csicsvari, J., Jamieson, B., Wise, K.D. and Buzsáki, G. (2003). Mechanisms of gamma oscillations in the hippocampus of the behaving rat. Neuron 37, 311-322.

Fujisawa, S., Amarasingham, A., Harrison, M.T., and Buzsáki, G. (2008). Behavior-dependent short-term assembly dynamics in the medial prefrontal cortex. Nat Neurosci. 11(7), 823-33.

Harris, K.D., Henze, D.A., Csicsvari, J., Hirase, H., and Buzsáki, G. (2000). Accuracy of tetrode spike separation as determined by simultaneous intracellular and extracellular measurements. J Neurophysiol. 84, 401-14.

Hazan, L., Zugaro, M., and Buzsáki, G. (2006). Klusters, NeuroScope, NDManager: a free software suite for neurophysiological data processing and visualization. J Neurosci Methods. 155, 207-16.

Mitra, P.P., and Pesaran, B. (1999). Analysis of dynamic brain imaging data. Biophys J. 76(2), 691-708.

Mizuseki, K., Diba, K., Pastalkova, E., and Buzsáki, G. (2011) Hippocampal CA1 pyramidal cells form functionally distinct sublayers. Nat Neurosci. 14, 1174-81.

Montgomery, S.M., Betancur, M.I., and Buzsáki, G. (2009). Behavior-dependent coordination of multiple theta dipoles in the hippocampus. J Neurosci. 29, 1381-94.

Paxinos, G., and Watson, C. (1996). The Rat Brain in Stereotaxic Coordinates, Compact 3rd Edition CDRom. Academic Press, San Diego.

Royer, S., Sirota, A., Patel, J., and Buzsáki, G. (2010). Distinct representations and theta dynamics in dorsal and ventral hippocampus. J Neurosci. 30, 1777-87.

Siapas, A.G., Lubenov, E.V., and Wilson, M.A. (2005). Prefrontal phase locking to hippocampal theta oscillations. Neuron. 46, 141-51.

Sirota A, Montgomery S, Fujisawa S, Isomura Y, Zugaro M, Buzsáki G. (2008). Entrainment of neocortical neurons and gamma oscillations by the hippocampal theta rhythm. Neuron. 60(4), 683-97.

Winson, J. (1974) Patterns of hippocampal theta rhythm in the freely moving rat. Electroencephalogr Clin Neurophysiol. 36, 291-301.